Original Article

Increased BST-2 expression by HBV infection promotes HBV-associated HCC tumorigenesis

Jun Zhang[1#], Baisong Zheng[1#], Xiaolei Zhou[1], Tianhang Zheng[1], Hong Wang[1], Yingchao Wang[2], Wenyan Zhang[1]

[1]Institute of Virology and AIDS Research, the First Hospital of Jilin University, Changchun, China; [2]Hepatobiliary Pancreatic Surgery, the First Hospital of Jilin University, Changchun, China

Contributions: (I) Conception and design: W Zhang, B Zheng; (II) Administrative support: Y Wang; (III) Provision of study materials or patients: Y Wang; (IV) Collection and assembly of data: J Zhang, B Zheng, X Zhou, T Zheng; (V) Data analysis and interpretation: B Zheng, H Wang; (VI) Manuscript writing: All authors; (VII) Final approval of manuscript: All authors.

[#]These authors contributed equally to this work.

Correspondence to: Yingchao Wang, Wenyan Zhang. The First Hospital of Jilin University. No 519 East Minzhu Avenue, Changchun 130021, China. Email: zhangwenyan@mail.jlu.edu.cn; yingchao11111@sohu.com.

Background: The majority of hepatocellular carcinoma (HCC) is closely associated with hepatitis B virus (HBV) infection, while the mechanism of HCC induced by HBV is debatable. Bone marrow stromal cell antigen 2 (BST-2), an N-glycoprotein, has been characterized as an oncogenic factor in several types of cancer. However, whether BST-2 plays an important role in HCC tumorigenesis remains unknown.

Methods: A total of 182 HCC tumorous and adjacent nontumor liver tissues were collected. HepG2, Huh7, L02, HepAD38, and HEK293T cell lines were adopted in this study. Tumor proliferation was detected by CCK8, transwell, wound healing, colony formation assays *in vitro*, and *in vivo* tumorigenesis was measured by mouse xenografts. NF-κB activation was determined by luciferase assay and Western blot. Protein expression was detected by Western blot, ELISA, or qPCR. Immunoprecipitation was used to confirm the interaction between BST-2 and Syk.

Results: Here, we observed the higher BST-2 expression in HBV-infected HCC than their paired adjacent tissues and HBV-uninfected HCC tissues, particularly more aberrant non-N-glycosylated BST-2 in HBV-infected HCC tumors. We also observed the increased ER degradation-enhancing α-mannosidase-like protein 3 (EDEM3), which is trimming of N-linked glycans by sequential removal of mannose residues, might result in more non-N-glycosylated form of BST-2. Moreover, we demonstrated that BST-2 and non-N-glycosylated BST-2 N65/92A mutant, not only enhanced the tumor characteristics of hepatoma cell lines *in vitro*, but also enhanced the growth of mouse xenografts *in vivo*. Mechanically, N65/92A mutant has stronger ability to promote HCC than BST-2 via NF-κB/ERK1/2 but not NF-κB/anti-apoptotic factors pathway. NF-κB inhibitor attenuated BST-2-mediated tumorigenesis of HCC.

Conclusions: Our findings illuminate the novel function of BST-2 as an oncogene of HBV-associated HCC, and highlight the novel relationship of N-glycosylation of BST-2 in regulating HCC tumorigenesis *in vitro*.

Keywords: Hepatitis B virus (HBV); hepatocellular carcinoma (HCC); bone marrow stromal cell antigen 2 (BST-2); N-glycosylation

Submitted Aug 26, 2020. Accepted for publication Jan 11, 2021.
doi: 10.21037/jgo-20-356
View this article at: http://dx.doi.org/10.21037/jgo-20-356

Introduction

Hepatocellular carcinoma (HCC), the sixth most common cancer and the fourth leading death of cancer, accounts for 80–90% of primary liver cancer around the world (1). HBV infection is the primary etiologic factor of HCC, and causes the majority of HCCs develop because of liver damage and cirrhosis induced by long-term chronic inflammatory (2). Due to the lack of specific symptoms in the early stage, a majority of patients diagnosed with HCC present with local progression or distant metastasis. Although there has been substantial progress in the treatment of HCC, the five year survival rate is only about 18% (3). Therefore, there is an urgent requirement for new potential therapeutic targets in HCC.

Better knowledge of the changes in gene expression that occur during carcinogenesis may lead to improvements in diagnosis, treatment, and prevention of cancer. Human bone marrow stromal cell antigen 2 (BST-2), also known as Tetherin/CD317/HM1.24, is a tumor-associated transmembrane N-glycoprotein that is overexpressed on the cell surface of various tumors and correlates with aggressive disease and poor prognosis (4,5). Overexpression of BST-2 was detected in gastrointestinal cancer (6). Knockdown of the BST2 gene inhibits gastric cancer cell growth, suggesting that BST-2 could be a useful therapeutic target for gastric cancer. Furthermore, BST-2 is overexpressed on multiple myeloma cells (7). Immunotherapy with a monoclonal antibody against BST-2 reduces tumor size and improves survival in a multiple myeloma mouse model (8). Such monoclonal antibody against BST-2 induces antibody-dependent cellular cytotoxicity, suggesting that it may be effective for a wide range of human malignancies. In addition, high levels of BST-2 have been reported in endometrial, ovarian, breast, and lung cancer (5,9-11). The molecular mechanisms of BST-2 promoting tumor progression include the regulation of DNA methylation (12), negative regulation of transforming growth factors (TGF-β) (13), induction of cytokines or anti apoptotic genes (14), and activation of NF-κB signaling pathway (15). However, the correlation between BST-2 and HCC has not yet been investigated.

BST-2 also acts as a well-identified viral restriction factor of HBV (16). Its expression is stimulated by HBV infection via the interferon (IFN) pathway (17). HBV infection hijacks the host endoplasmic reticulum (ER) to produce a large quantity of viral glycoproteins (LHBs, MHBs, and SHBs), resulting in ER stress (18). This stress activates a series of quality control enzymes in cells to reduce the aberrant proteins in the ER by increasing protein folding, translation, and degradation. Among them, ER degradation-enhancing α-mannosidase-like (EDEM) protein can accelerate ERAD of misfolded glycoproteins. EDEM contains EDEM1, EDEM2, and EDEM3. Previous study reported that EDEM3 greatly stimulates mannose trimming and ERAD (19). In addition to trimming viral glycoproteins, EDEMs also trim cellular N-glycoproteins and are closely associated with cancer progression. Accumulating evidences showed that alterations in glycosylation patterns regulated cancer development and progression, serve as important biomarkers, and provide a set of specific targets for diagnosis and therapeutic intervention (20). N-linked glycan modification of proteins has been implicated in different kinds of cancers (21). BST-2 contains two N-linked glycosylation sites (Asn^{65} and Asn^{92}), which contribute to the double-N-glycosylated form (~30 kD), single-N-glycosylated form (~25 kD), and the non-N-glycosylated form (~20 kD) (22). Although mature BST-2 is highly glycosylated, the contribution of N-glycans to BST-2 function remains unknown.

Our previous study found that BST-2 expression might be associated with the tumorigenesis of HCC. We speculated that HBV infection induced BST-2 expression to promote HCC progression. And HBV induced EDEMs by ER stress would trigger the trimming of BST-2 N-glycan. Our objectives are to illuminate the relationship between BST-2 expression and HCC, and the contribution of N-glycans modification to BST-2 function. We believe that our findings will expand the current understanding of BST-2 functions in tumor development, and might explore novel therapeutic target of HCC. We present the following article in accordance with the ARRIVE reporting checklist (available at http://dx.doi.org/10.21037/jgo-20-356).

Methods

Patients and tumor tissue collection

A total of 182 HCC tumorous and adjacent specimens were acquired from the department of Biobank, the division of clinical research for the providing of human tissues of the First Hospital of Jilin University, including 45 HBV-infected HCC tumor tissues (clinically malignant tissues), 45 HBV-infected HCC adjacent tissues (clinically benign tissues), 46 HBV-uninfected HCC tumor tissues (clinically malignant), and 46 HBV-uninfected HCC adjacent tissues (clinically benign tissues). All the specimens were obtained

from clinical surgery for HCC patients occurred between August 2016 and March 2018. Only patients who had not undergone preoperative radiotherapy or chemotherapy and without clinical evidence of distant metastasis were enrolled in the study. A small tissue fraction (~100 mg/each) was taken for analysis. Samples were stored at −80 ℃ until dispersion. In our study, liver tissue up to 3 cm from the HCC tumorous tissue was defined as adjacent tissue. Characteristics of HCC patients are listed in *Table 1*.

Plasmids, antibodies, and reagents

BST-2 with an HA tag and the pCMV-HBV proviral plasmids were constructed as previously described (23). Mutants (N65A, N92A, and N65/92A) were cloned based on BST-2 HA with site-directed mutagenesis. The Syk, EDEM1, EDEM2, and EDEM3 gene with a Myc tag was amplified from the cDNA of healthy human peripheral blood mononuclear cells (PBMCs) and then was cloned into the eukaryotic expression vector VR1012.

The primary antibodies used in this study are listed in Table S1. The selective inhibitor MG132 (#M7449), and cycloheximide (CHX, #01810) were purchased from Sigma (St. Louis, MO, USA), and tetracycline, BAY 11-7082 (#S2913) was purchased from Selleck (Houston, TX, USA).

Cells and transfection

HepG2 [77400], Huh7, HepAD38, L02, and HEK293T (CRL-11268) cells were purchased from the ATCC, and they were cultured in DMEM supplemented with 10% serum at 37 ℃/5% CO_2. DNA transfection was performed using Lipofectamine 2000 (Life Technologies). Stable cell lines constitutively expressing BST-2 WT or mutant N65/92A were obtained using a lentivector-mediated gene transfer system that was combined with puromycin selection. Cell transfection with the vector plvx served as a blank control.

Immunohistochemical staining (IHC staining)

Sections from the HCC specimens and xenografts from the nude mice were fixed, sectioned, and heated; then, they underwent antigen retrieval, were incubated with the appropriate antibodies, dehydrated, and transparently sealed, and were finally prepared for immunohistochemical staining. Immunohistochemical staining using an anti-BST-2 antibody or anti-p65 antibody was performed;

Table 1 Characteristics of HCC patients in this study

Characteristic	Datum for patients	
	HBV-infected HCC (n=45)	HBV-uninfected HCC (n=46)
Gender		
Female	14 (31.1)	17 (37.0)
Male	31 (68.9)	29 (63.0)
Age, years	51.2±14.7	49.6±17.3
HBV viral load (IU/mL)	3,522±1,266	<50
Antiviral therapy	No	No
Specimens obtain	Surgery	Surgery
AFP, μg/L	11,425±12,451	18,042±4,235
GGT, U/L	74.9±77.3	89.4±63.7
Liver cirrhosis		
No	20 (44.4)	26 (56.5)
Yes	25 (55.6)	20 (43.5)
Tumor size, cm	7.5±3.5	6.4±4.4
Tumor number		
Solitary	40 (88.9)	33 (71.7)
Multiple	5 (11.1)	13 (28.3)
Vascular invasion		
No	32 (71.1)	31 (67.4)
Yes	13 (28.9)	15 (32.6)
Tumor capsule		
No/incomplete	33 (73.3)	37 (80.4)
Complete	12 (26.7)	9 (19.6)
Differentiation grade*		
I + II	6 (13.3)	9 (19.6)
III + IV	39 (86.7)	37 (80.4)
TNM stage		
I	16 (35.6)	15 (32.6)
II–IV	29 (64.4)	31 (67.4)
BCLC stage		
0–A	39 (86.7)	33 (71.7)
B–C	6 (13.3)	13 (28.3)
Recurrence		
No	21 (46.7)	14 (30.4)
Yes	24 (53.3)	32 (69.6)
BST-2 expression		
Low	25 (55.6)	4 (8.7)
High	20 (44.4)	42 (91.3)

Values are expressed as the mean ± SD or n (%), unless otherwise indicated. *, according to the Edmondson and Steiner grading system. AFP, alpha-fetoprotein; GGT, gamma-glutamyl transferase.

results were scored and analyzed separately.

Western blot analysis

Cells were harvested and lysed in radio immune precipitation assay lysis buffer (50 mM Tris-HCl (pH 7.5), 150 mM NaCl, and 1% NP-40), and the lysate was cleared by centrifugation at 16,000 ×g at 4 ℃ for 5 min. The total cell extracts were subjected to SDS-PAGE and then were transferred onto nitrocellulose membranes (#10401196; Whatman). After blocking with 5% nonfat dry milk in Tris-buffered saline with Tween (TBST) for 1 h, the membranes were incubated with the indicated primary antibodies and then with the corresponding alkaline phosphatase (AP)-conjugated secondary antibodies (Sigma) for 1 h. After three washes with TBST, the blots were reacted with nitro blue tetrazolium (NBT) and 5-bromo-4-chloro-3'-indolylphosphate (BCIP) (Sigma).

RNA extraction and qRT-PCR

RNA isolation and real-time qRT-PCR were performed by following the MIQE guidelines (24). Total RNA was extracted from the tumor tissues and xenografts with TRIzol reagent. Then, the RNA was reverse transcribed using Transcriptor cDNA Synthesis kit 1 (#4896866001, Roche, Basel, Switzerland). qRT-PCR was carried out on an Mx3005P instrument (Agilent Technologies, Stratagene, USA) by using a master mix (SYBR green) kit (Bio-Rad) and the primers listed in Table S2. qRT-PCR assays were carried out in a 20 μL volume consisting of 10 μL of a 2× SYBR green mix solution, 0.4 μL of each oligonucleotide primer (5 μM), and 2 μL of the cDNA template. The target fragment amplification was carried out as follows: 50 °C for 2 min and 95 ℃ for 10 min, followed by 50 cycles of 95 ℃ for 15 s and 60 ℃ for 1 min. A melting curve analysis was carried out at 90 ℃ for 1 min, 55 ℃ for 30 s and 95 ℃ for 30 s. qbase + software (Biogazelle) was applied to characterize the expression stability of three reference genes (β-actin, GAPDH, and HMBS) (25), and these genes showed high reference target stability (geNorm M <0.5). To minimize the bias that may be caused by heterogeneity of HCC patients, BST-2 or EDEM1, 2, 3 expression in HCC patients was calculated by normalization with the geometric means of the three reference genes. Primers for real-time qRT-PCR are listed in Table S2. For anti-apoptosis factors, Bcl-xL, CIAP2, FLIP, and livin in xenograft tumors, the threshold cycle value of each sample was calculated, and the relative mRNA level was normalized to the mRNA level of GAPDH.

Cell proliferation analysis

Cells were seeded at a density of 1.0×10^3 cells per well of 96-well plate. At the time points of 0, 1, 2, and 3 days, cell proliferation was assayed using a CCK8 kit (#FC101, TransGen) according to the manufacturer's instructions.

Wound healing assay

Cells were inoculated into 6-well plates at densities of 5×10^5 cells per well. After cells covered the bottom of the plate, a pipette was used to make a scratch in the wells of cells, and each scratch had the same width. The well was rinsed, and the cell debris was removed. The culture plates were placed in an incubator to continue incubating, and photographs were taken.

Transwell cell migration assays

5×10^5 cells were resuspended in serum-free media and were seeded into an upper transwell chamber, while FBS-containing media was added to the bottom chamber to provide chemoattractant for migration. After 24 h, the migrated cells were fixed with methanol and then were stained with crystal violet for cell counting.

Colony formation assay

The cells were seeded in 6-well plates at a density of 500 cells/well and were then incubated with DMEM with 10% FBS at 37 ℃. Two weeks after seeding, the cells were fixed and stained with 0.1% crystal violet, and the number of colonies was examined under a light microscope.

Xenograft analysis

1.0×10^6 cells were suspended in DMEM medium and were injected subcutaneously into the flank of 6-week-old female nude mice (n=5). Mice were housed in laminar flow cabinets under specific pathogen-free conditions at room temperature with a 24 h night/day cycle and ad libitum access to food pellets and water. The tumors were dissected and weighed at the end of the experiment. RNA and protein samples from the tumors were purified for gene expression analysis.

Luciferase assay for assessing NF-κB activation

Cells were transfected with BST-2, an HBV expression plasmid, a pNF-κB-Luc reporter plasmid (Agilent) and a Renilla luciferase plasmid as an indicator of transfection. After two days, the activities of firefly luciferase and Renilla luciferase were examined with a dual-luciferase reporter assay system (Promega) according to the manufacturer's instructions. Firefly luciferase activity was normalized to Renilla luciferase activity.

Immunoprecipitation

Ten-cm dishes of HEK293T cells were transfected with pCDNA3.1 BST-2 WT and mutants with the VR1012 Syk construct. After 48 h of transfection, cells were harvested and lysed with buffer containing a protease inhibitor cocktail. Cell lysates were incubated with an anti-Myc antibody and protein G agarose beads (Life Technologies) at 4 ℃ overnight. After washing, the proteins were eluted, and the eluted proteins were obtained by centrifugation, which was followed by SDS-PAGE and WB analysis.

Kaplan-Meier analysis

The prognostic value of mRNA expression of BST-2 in liver cancers was analyzed by using Kaplan-Meier analysis in GraphPad Prism. HBV-infected HCC patients were divided into high and low of BST-2 expression group based on median values of mRNA expression and validated by K-M survival curves. Statically significant difference was considered when a P value <0.05.

Statistical analysis

The statistical analyses were performed with GraphPad Prism version 8.2.1 (GraphPad Software Inc., La Jolla, CA, USA). The results are expressed as the median, percent or mean ± standard deviation. The difference among HBV-infected and HBV-uninfected specimens were analyzed by one-way ANOVA. The differences between the benign and malignant specimens were analyzed by means of unpaired Student's *t*-tests or Mann-Whitney U tests. Finally, P<0.05 was considered indicative of a significant difference.

Ethical statement

The study was conducted in accordance with the Declaration of Helsinki (as revised in 2013). The study was approved by the Ethics Review Boards of the First Hospital of Jilin University (No. 2016-255) and informed consent was taken from all individual participants.

For any experiments involving animals, they were performed under a project license (No. 2016-320) granted by the Institutional Animal Care and Use Committee (IACUC) of Jilin University, in compliance with Chinese national or institutional guidelines for the care and use of animals. All procedures used in the animal studies were approved by All animal experiments met the Animal Welfare guidelines.

Results

BST-2 expression is upregulated in HBV-associated HCC

Our team previously identified that BST-2 acts as a viral restriction factor of HBV, since it can tether the HBV virion on the cell membrane (23). However, as an IFN-inducible protein, BST-2 could not limit the replication of HBV. Here, we observed that the increasing dose of HBV expression enhanced BST-2 expression in HepG2 cells in dose-dependent manner (*Figure 1A*). Meanwhile BST-2 but not HBV activated the nuclear factor κB (NF-κB) signaling in cells (*Figure 1B*). We speculate that HBV-induced BST-2 expression may involve in HCC tumorigenesis by NF-κB activation. Hence, we investigated the clinical relevance of the BST-2 expression in HBV-infected or HBV-uninfected HCC tumorous compared to their adjacent tissues. Characteristics of enrolled HCC patients are listed in *Table 1*. As shown in *Figure 1C*, BST-2 mRNA levels were higher in 45 HBV-infected HCC tumors than their adjacent tissues and 46 paired HBV-uninfected HCC specimens. No differences on BST-2 mRNA levels were detected between 46 HBV-uninfected HCC tumors and their adjacent tissues. Immunohistochemical analysis showed that more dark brown plaques of endogenous BST-2 were presented in HBV-infected HCC tumors than in adjacent tissues. However, BST-2 expression was no difference between HBV-uninfected HCC tumors and their adjacent specimens (*Figure 1D*). In order to confirm the induction effect of HBV on BST-2 expression, endogenous BST-2 expression was detected by Western blot after HBV transfection. The results indicated that HBV also induced stronger endogenous BST-2 expression in HepG2 cells (*Figure 1E*). In addition, HepAD38 and HEK293T cells were pretreated with tetracycline for 72 h, then tetracycline was removed,

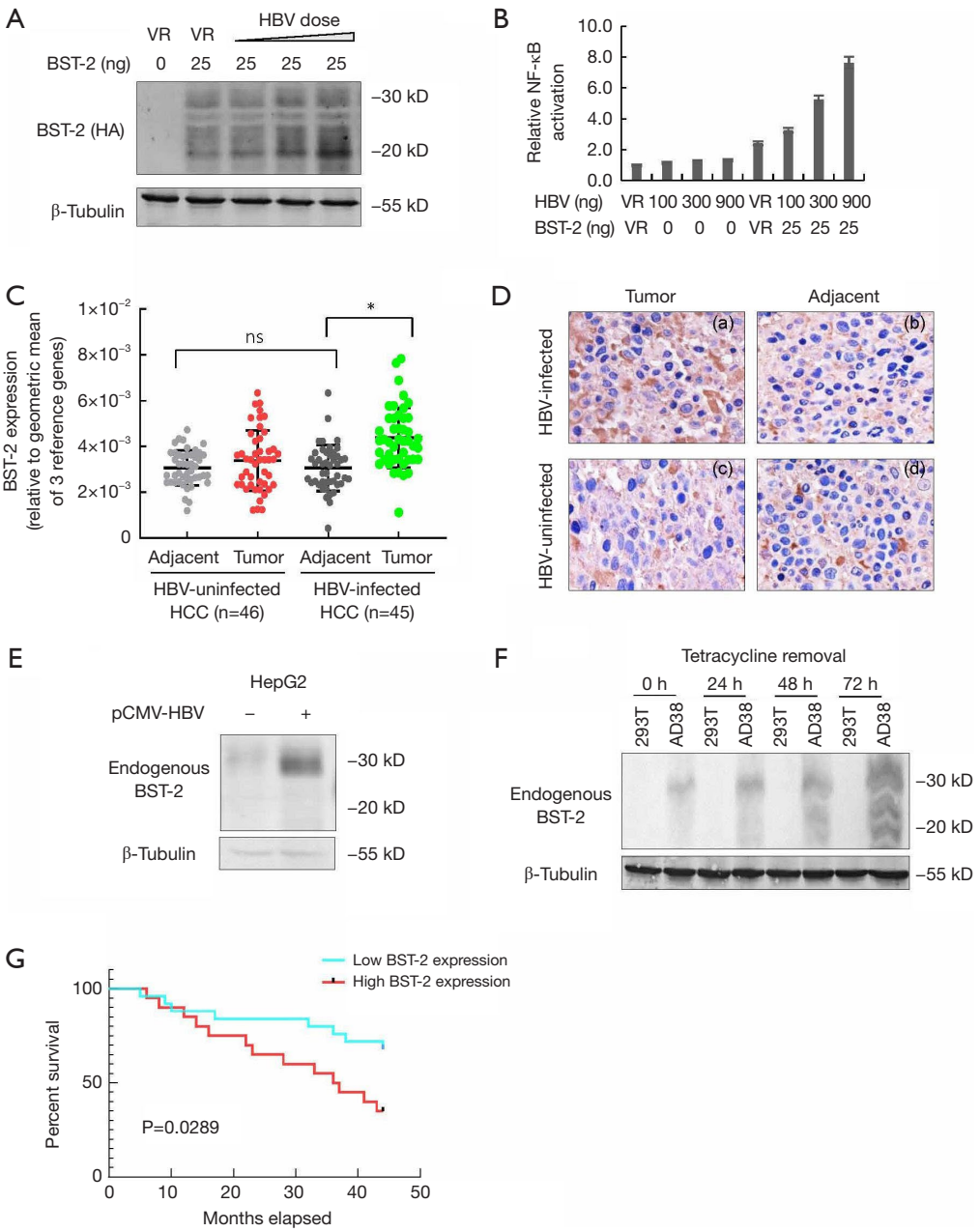

Figure 1 HBV induced BST-2 expression in HBV-infected HCC. (A) The BST-2 with increasing amounts of pCMV-HBV viral vector (0, 100, 300, and 900 ng) was cotransfected into HEK293T cells as indicated. After 48 h, cells were harvested. BST-2 expression in cell lysate was determined by Western blot. (B) pNF-κB-Luc reporter plasmid and Renilla luciferase plasmid were cotransfected with BST-2 and pCMV-HBV plasmids into HEK293T cells as indicated. NF-κB activation was determined by a dual-luciferase reporter assay at 48 h after transfection. (C) RNA levels of BST-2 in HCC tumors and adjacent tissues were detected by qRT-PCR. The geometric means of the β-actin, GAPDH, and HMBS genes were used for normalization. (D) Immunohistochemical analysis of BST-2 expression in paired HBV-infected or HBV-uninfected human HCC tumorous tissue and adjacent tissues. Representative images of tumor (left) and adjacent tissue (right) are shown (×100). (E) pCMV-HBV viral vector was transfected into HepG2 cells. Endogenous BST-2 expression was detected by Western blot. (F) HepAD38 cells were pretreated with tetracycline for 72 h, and then tetracycline was removed. BST-2 expression in HepAD38 was detected by Western blot for 72 h. HEK293T cells were used as negative control. (G) The prognostic value of mRNA expression of BST-2 in liver cancers was analyzed by using Kaplan-Meier analysis in GraphPad Prism. Liver tissue up to 3 cm from the HCC tumorous tissue was defined as adjacent tissue. ns, no significance; *, P<0.05.

HBV-producing HepAD38 cells but not HEK293T cells will produce and secrete HBV. With HBV secretion, BST-2 expression in HepAD38 cells was enhanced gradually in time-dependent manner (*Figure 1F*). To demonstrate the clinical importance of BST-2 expression, patient survival of HBV-infected HCC was analyzed by Kaplan-Meier curve. The result demonstrated that high BST-2 expression accelerated the death of HBV-infected HCC patients. These data suggested that HBV-induced BST-2 expression might be a relevant factor in HBV-infected HCC tumorigenesis.

HBV induces aberrant expression of non-N-glycosylated BST-2

Transient transfected expression of BST-2 usually contains three forms corresponding to the double-N-glycosylated (~30 kD), the single-N-glycosylated (~25 kD), and the non-N-glycosylated form BST-2 (~20 kD) (*Figure 2A*). We observed that HBV also enhanced the expression of BST-2 mutants N65A, N92A and N65/92A, which represent different N-glycosylated forms of BST-2 in HEK293T cells (*Figure 2B*). To further investigate the effect of HBV on N-glycosylated form of BST-2, we detected the endogenous BST-2 expression in paired HBV-infected HCC samples by Western blotting. Double-N-glycosylated BST-2 was observed in the adjacent tissues of HBV-infected HCC tumors, while only non-N-glycosylated BST-2 was observed in the HBV-infected HCC tumor samples (*Figure 2C*). However, the expression pattern of BST-2 was not changed in HBV-uninfected HCC tumors and adjacent tissues (*Figure 2D*). This result suggested that HBV might induce aberrant expression of non-N-glycosylated BST-2 in HBV-infected HCC tumors.

HBV-induced EDEM3 promotes the trimming of glycoprotein BST-2

HBV hijacks the host endoplasmic reticulum (ER) to produce a large quantity of viral glycoproteins resulting in ER stress (18). This stress activates a series of protein quality control enzymes, including EDEM1, 2, and 3, to reduce the quantity of aberrant proteins. Previous studies have demonstrated that EDEMs, which are responsible for N-glycan trimming from glycoprotein, could be induced by LHBs (26). Here, we investigated the transcription of EDEMs in 45 paired HBV-infected HCC samples by qRT-PCR. Statistical analysis showed that EDEM2 and EDEM3 but not EDEM1 were upregulated in HBV-infected HCC tumors (*Figure 3A*). TCGA dataset also revealed the relevance between the increased expression of EDEM2, EDEM3 and HCC tumorigenesis (data not shown).

To investigate the effect of EDEM3 on N-glycan trimming, EDEM 3 was transfected with BST-2 WT or indicated mutants into HEK293T cells. Western blot showed that for BST-2 WT, the double-N-glycosylated BST-2 was decreased and the non-N-glycosylated BST-2 was increased in the presence of EDEM3, whereas EDEM3 resulted in the decreased expression levels of for BST-2 mutants (*Figure 3B*). Deglycosylation and proteasomal degradation of BST-2 were spontaneously controlled by the ER-associated degradation (ERAD) (27). CHX chase assay was applied to monitor the turnover of different forms of BST-2 by inhibiting *de novo* protein synthesis. Compared with the WT, N-glycosylation deficiency of BST-2 increased the rate of degradation for all mutants, especially the N65/92A mutant. Interestingly, HBV recovered the degradation of N-glycosylation deficient mutants (*Figure 3C*). Since BST-2 and N-glycosylation deficiency mutants can tether HBV by interact with HBV envelope (23,28), we speculate that HBV can enhance the stability of N-glycosylated deficient BST-2, especially non-N-glycosylated BST-2. To verify our thoughts, proteasome inhibitor MG132 was used to block the degradation of BST-2. As shown in *Figure 3D*,*E*, the presence of HBV obviously increased the production of non-N-glycosylated BST-2 rather than the WT, suggesting that HBV induces N-glycan trimming of BST-2 by EDEM3, and extends the turnover time of N-glycan deficient BST-2 *in vitro*.

Non-N-glycosylated of BST-2 enhances HCC tumorigenesis more in vitro and in vivo than BST-2

Based on the HBV-infected HCC specimen, we found that non-N-glycosylated BST-2 was aberrantly overexpressed in HCC tissues by HBV-induced EDEM3 (*Figure 2C*). To unveil the effect of non-N-glycosylated BST-2 on HCC tumorigenesis, stable hepatocyte cell lines expressing WT BST-2 and mutant N65/92A were constructed and briefly termed as HepG2:WT, Huh7:WT, HepG2:N65/92A, and Huh7:N65/92A. Cell proliferation showed that HepG2:N65/92A and Huh7:N65/92A exhibited increasing growth rates compared to those of the HepG2:WT, Huh7:WT, and control cells (*Figure 4*). Wound healing assay showed that BST-2 N65/92A expression rescued the wound closure faster than WT and the control (*Figure 4B*,*F*).

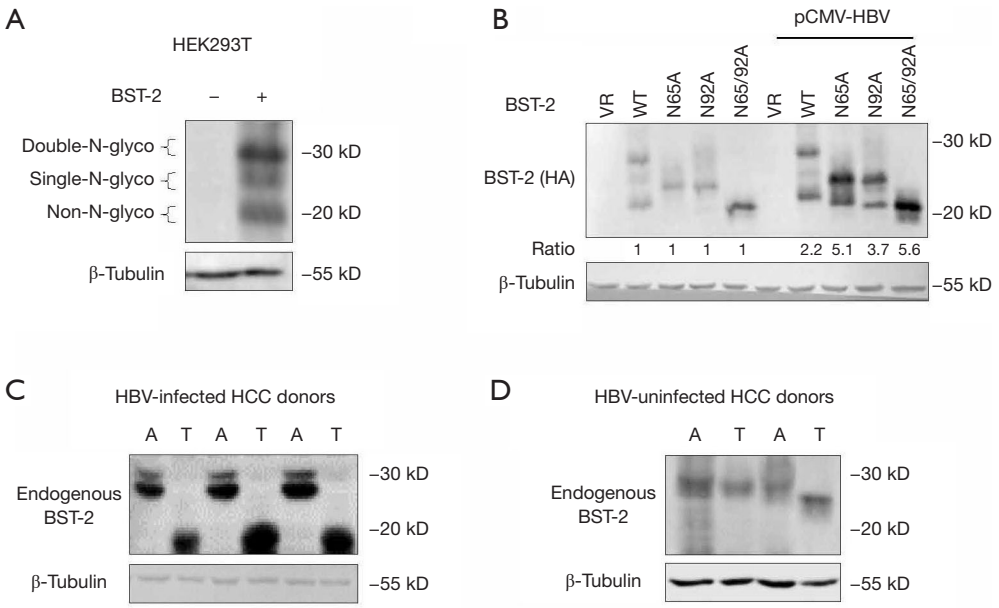

Figure 2 More aberrant N-glycosylation of BST-2 was observed in HBV-infected HCC. (A) Western blot analyses detected the expression of BST-2 WT in transient transfected HEK293T cells. (B) WT and mutant BST-2 were cotransfected with/without pCMV-HBV viral vector into HEK293T cells. Western blot detected the expression of WT and mutant BST-2 expression in cells. (C) Western blot analyses showing endogenous BST-2 expression in paired HBV-infected HCC tissues. (D) Western blot analyses showing endogenous BST-2 expression in paired HBV-uninfected HCC tissues. A, adjacent tissue; T, tumor tissue.

However, statistical analysis showed that mutant N65/92A endowed cells with weak enhancement of migration ability than WT and control cells. Cell invasion ability was evaluated by transwell assay. As shown in *Figure 4C,G*, the cell invasion ability was ordered as follows: HepG2:N65/92A or Huh7:N65/92A > HepG2:WT or Huh7:WT > control cells. In addition, mutant N65/92A enhanced colony formation ability (colony number or colony size) of cells comparing with WT and control (*Figure 4D,H*). In order to exclude the influence of the experimental cell line we used to the results, normal hepatocytes L02 were used to investigate the function of BST-2. The results of cell proliferation, would healing, and colony formation demonstrated that BST-2 and mutant N65/92A could enhance tumor characteristics of L02 cells (Figure S1). These findings demonstrated that BST-2, particularly non-N-glycosylated BST-2, could enhance the proliferation, invasion, and colony formation ability of hepatocyte cells *in vitro*. Mouse xenograft model was performed to evaluate the effect of BST-2 on HCC tumorigenesis *in vivo*. Consistent with the *in vitro* results, BST-2 mutant N65/92A significantly promoted the formation and growth of xenografts than the WT and control. Meanwhile, WT BST-2 expression also enhanced HCC tumorigenesis *in vivo* (*Figure 4I*).

BST-2 functions in HCC tumorigenesis via the NF-κB/ERK pathway

Accumulated evidence suggests that NF-κB is activated in HBV-induced hepatitis, and it is causally associated with subsequent inflammation-driven HCC (29,30). BST-2, depending on a conserved tyrosine motif on its cytoplasmic tail, exactly activates NF-κB leading to the expression of both proinflammatory cytokines and proteins involved in cell survival (31,32). Therefore, we investigated the effect of BST-2 N-glycosylation on NF-κB activation. As shown in *Figure 5A*, WT BST-2 weakly activated the NF-κB, whereas the mutant N65/92A strongly activated NF-κB. In cooperation with HBV, the mutant N65/92A remarkably activated the NF-κB ~100-fold over the control (*Figure 5B*). These findings have given rise to much speculation that N-glycosylation of BST-2 may involve in HBV-associated HCC via the NF-κB pathway. Spleen tyrosine kinase (Syk) can be recruited by conserved tyrosine motif of BST-2 for downstream NF-κB activation (32). Syk

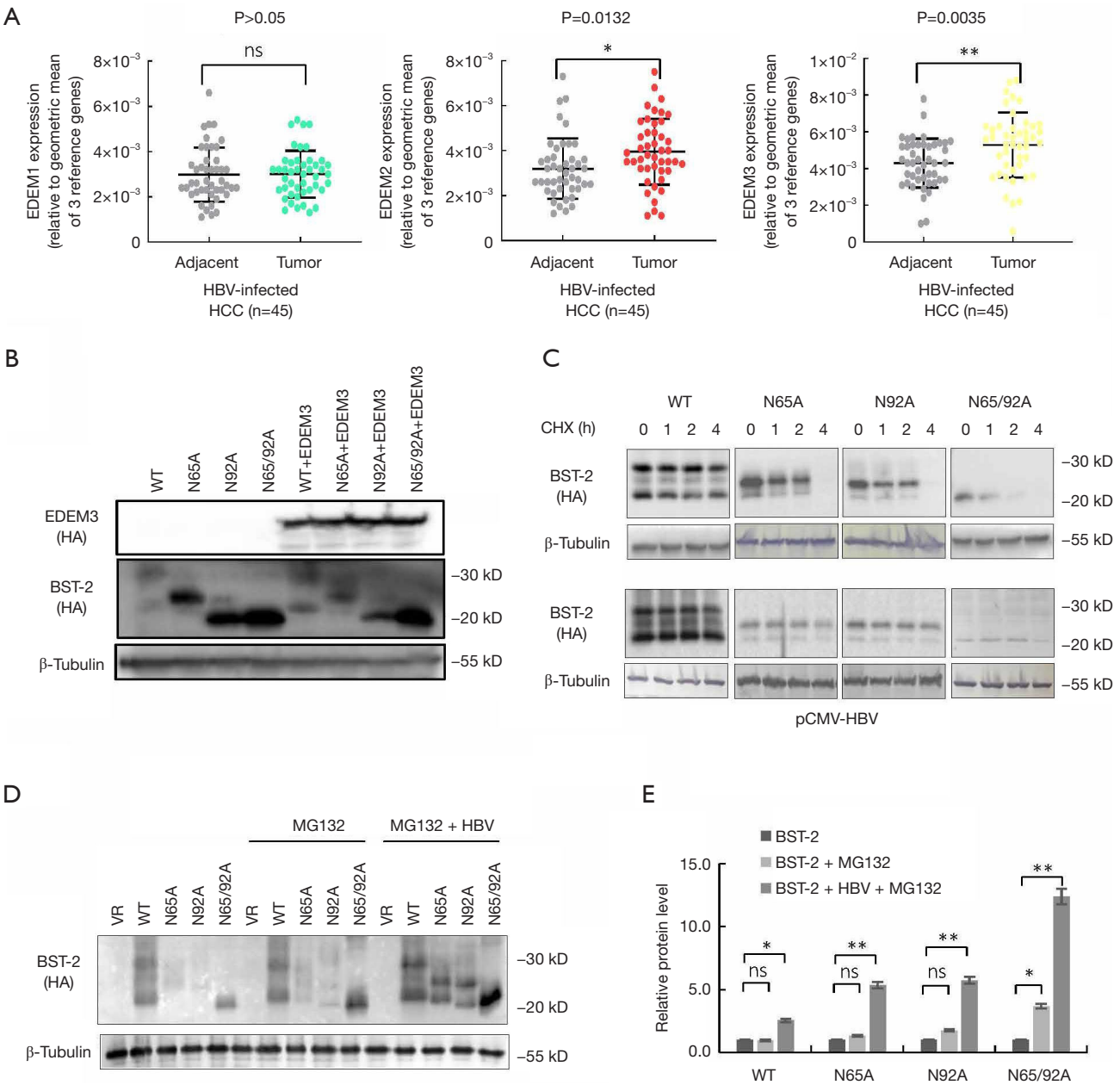

Figure 3 HBV-induced EDEM3 promotes the N-glycan trimming of BST-2. (A) RNA levels of EDEM1, EDEM2, and EDEM3 in HBV-infected HCC tumors and adjacent tissues were detected by qRT-PCR. The geometric means of the β-actin, GAPDH, and HMBS genes were used for normalization. (B) The effect of EDEMs on the expression of different N-glycosylated BST-2. (C) CHX chase assays detected the degradation of WT BST-2 and mutants N65A, N92A, N65/92A. (D) Western blot analyses showing the expression of BST-2 WT and mutants N65A, N92A, N65/92A in the presence of the proteasome inhibitor MG132. ns, no significance; *, P<0.05; **, P<0.01. (E) Relative protein levels analyses according to D by Image J.

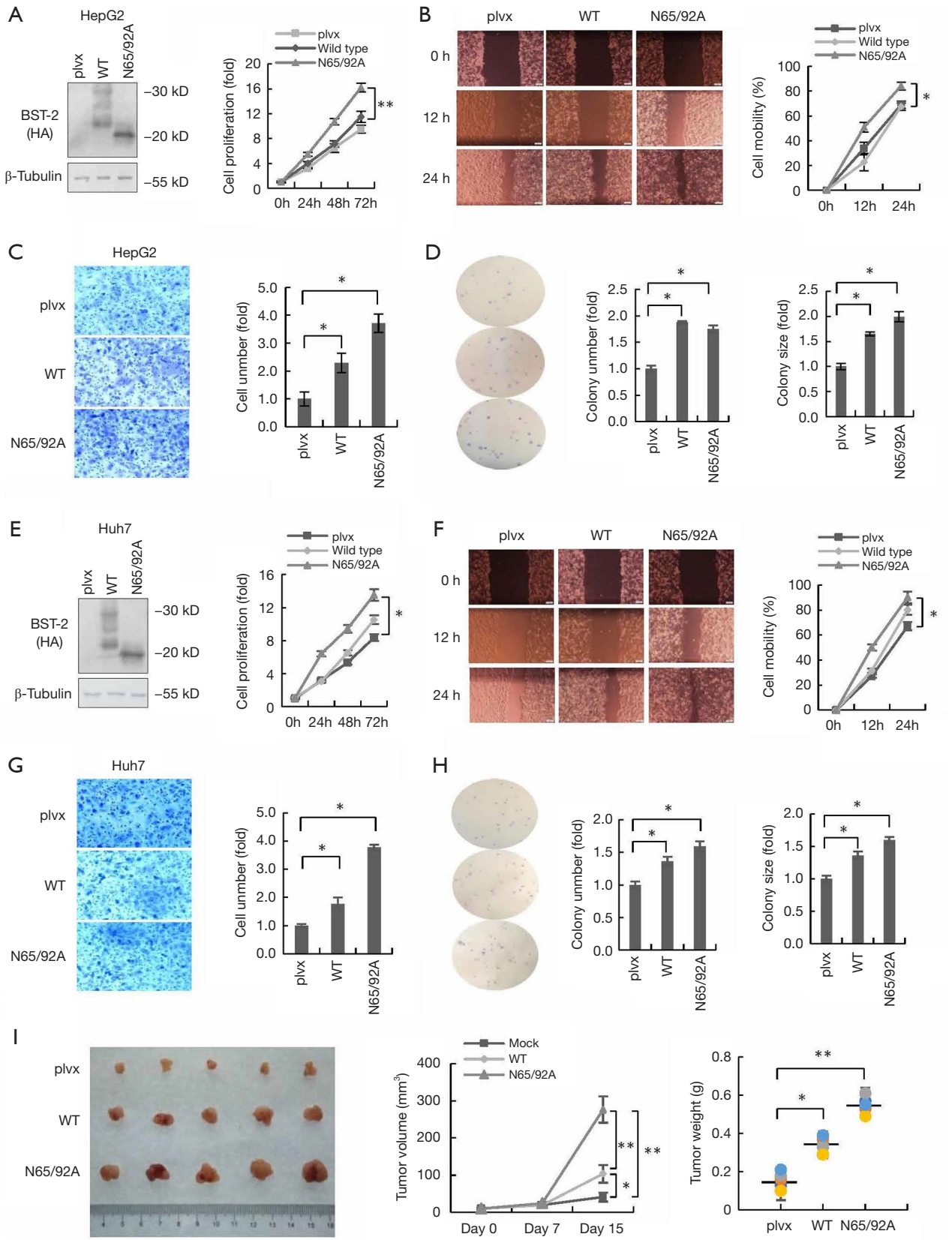

Figure 4 N-glycosylation of BST-2 involves HCC tumorigenesis *in vitro* and *in vivo*. (A) BST-2 was detected in stably transfected HepG2 cell line by western blot. Cell proliferation of HepG2:WT, HepG2:N65/92A, and control cells was measured by CCK8. (B) Cell migration of HepG2:WT, HepG2:N65/92A, and control cells was measured and quantified by wound healing assays (×10). (C) Invasion of HepG2:WT, HepG2:N65/92A, and control cells was measured and quantified by transwell assays (×50). (D) Colony formation of HepG2:WT, HepG2:N65/92A, and control cells was measured and quantified. (E) BST-2 was detected in stably transfected Huh7 cell line by western blot. Cell proliferation of Huh7:WT, Huh7:N65/92A, and control cells was measured by CCK8 assays. (F) Cell migration of Huh7:WT, Huh7:N65/92A, and control cells was measured and quantified by wound healing assays (×10). (G) Invasion of Huh7:WT, Huh7:N65/92A, and control cells was measured and quantified by transwell assays (×50). (H) Colony formation of Huh7:WT, Huh7:N65/92A, and control cells was measured and quantified. (I) The effects of BST-2 WT and mutant N65/92A on HCC tumor growth and proliferation in an SCID mouse model. Five mice were used for each group. The volume of tumors was measured at different time points, as indicated. Tumors were excised and weighed after 15 days of injection. The results are reported as the mean ± SD of three independent experiments. ns, no significance; *, P<0.05; **, P<0.01.

immunoprecipitation was performed in the presence of WT BST-2 and mutant N65/92A. The results showed that mutant N65/92A displayed a stronger interaction with Syk than WT BST-2 (*Figure 5C*). This result revealed the mechanism by which non-N-glycosylated BST-2 induced excessive NF-κB activation.

Several studies have proved that BST-2 involves in some kinds of tumors by controlling cell survival pathways, such as ERK1/2 or AKT (33,34). Here, western blot verified that BST-2 and N65/92A mutant strongly increased the total p65 and phosphorylated IκBα than the control in mice xenografts, and N65/92A mutant increased more than WT (*Figure 5D*). Furthermore, NF-κB activation resulted in the upregulation of phosphorylated ERK1/2, which is a downstream cell proliferation pathway, but there was no effect on total AKT or phosphorylated AKT (*Figure 5E*). To rule out other possibilities, the mRNA levels of four typical anti-apoptosis factors, Bcl-xL, CIAP2, FLIP, and livin, in xenograft tumors were assessed by qRT-PCR. All four anti-apoptosis factors were not regulated by either WT BST-2 or the mutant N65/92A (*Figure 5F*). This evidence indicated that non-N-glycosylated BST-2 might stimulate NF-κB/ERK1/2 signaling but not anti-apoptosis factors to promote cell survival.

NF-κB inhibition attenuates the promotion of HCC by BST-2

A specific NF-κB inhibitor (BAY 11-7082) was employed to confirm the mechanism of BST-2 and non-N-glycosylated BST-2-induced tumorigenesis in HCC. BAY 11-7082 (10 nM)-treated or untreated HepG2 cells were transfected with BST-2 and HBV expression plasmids. As shown in *Figure 6A*, 10 nM BAY 11-7082 mostly blocked NF-κB activation of WT BST-2 or mutant N65/92A. Then, the cell proliferation (*Figure 6B*), migration (*Figure 6C*), and colony formation (*Figure 6D*) of three stable HepG2 cell lines (control, HepG2:WT, HepG2:N65/92A) were assessed following pretreated with or without the inhibitor. Consistent with the results in *Figure 4*, BST-2 and N65/92A mutant induced HepG2 cells to exhibit characteristics of tumor progression in the untreated group. However, inhibitor treatment attenuated the effect of BST-2 in promoting tumor progression. This indicated that BST-2 and non-N-glycosylated BST-2 induced tumorigenesis by excessive NF-κB activation *in vitro*.

Discussion

HBV chronic infection causes more than half of HCC cases (35,36). Previous studies reported that BST-2 as a host restrictive factor can inhibit HBV spreading by tethering the nascent viruses to the surface of the infected cells (37,38), but can not kill virus. Moreover, BST-2 can activate the NF-κB signal, which may lead to cell survival (31,32,39). However, the relevance of BST-2 and HCC progression remains unclear. Since HBV infection is an important factor for HBV-associated HCC, we investigated BST-2 expression in paired HBV-infected or HBV-uninfected HCC specimens (*Figure 1*). Compared to HBV-uninfected HCC tumors, more BST-2 was expressed in HBV-infected HCC tissues than that in paired adjacent tissues. Increasing dose of HBV over-transfection also promoted BST-2 expression, further confirming that HBV is closely associated with the increased BST-2 levels, which is consistent with previous study that BST-2 expression is stimulated by HBV infection via IFN pathway (17). On the other hand, our results suggest BST-2 may play an

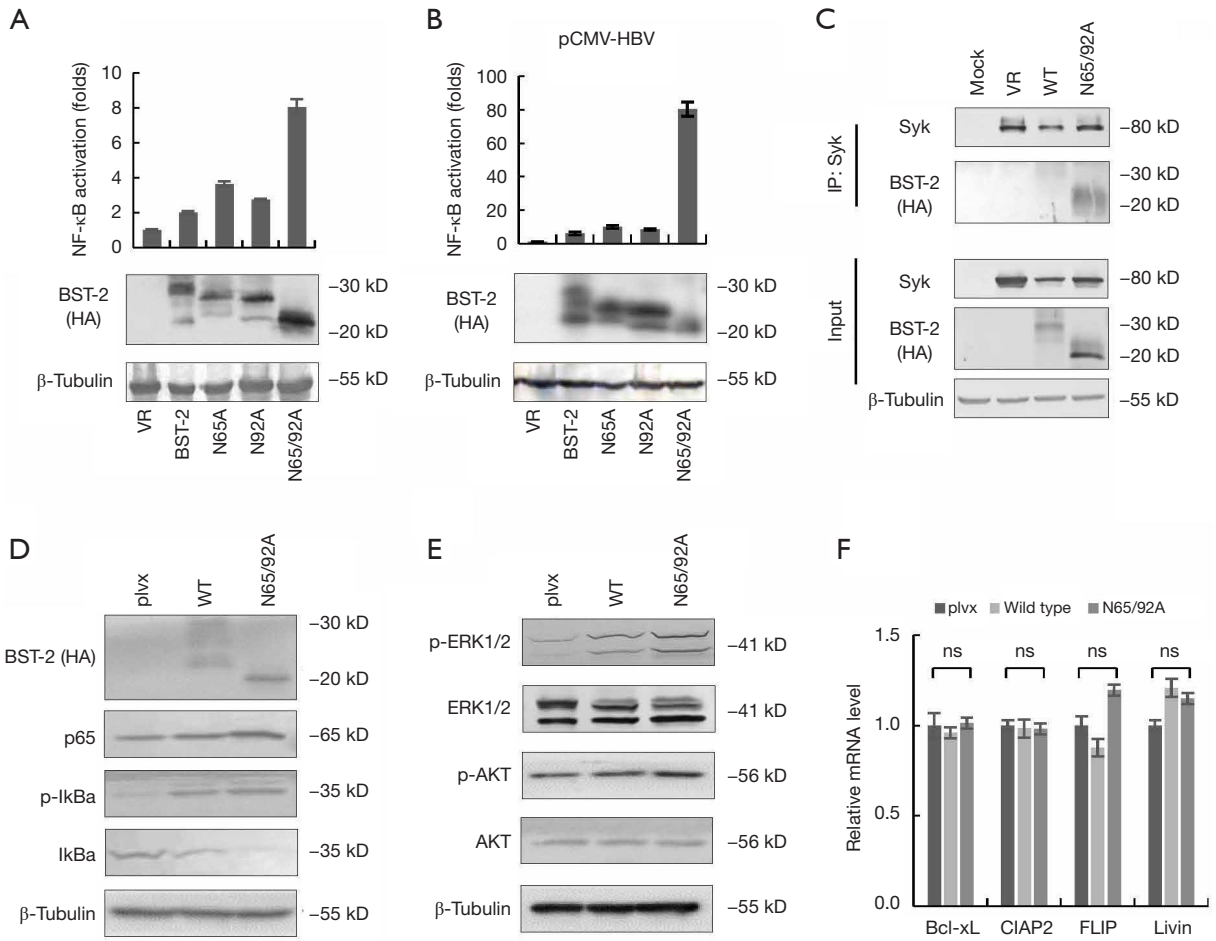

Figure 5 N-glycosylation of BST-2 regulates NF-κB/ERK activation. (A) The effect of WT BST-2 and its mutants on NF-κB activation was measured by dual-luciferase reporter assays. (B) The effect of WT BST-2 and its mutants on NF-κB activation was measured in the presence of HBV by dual-luciferase reporter assays. (C) Immunoprecipitation assay detecting the interaction between BST-2 and Syk. (D) Western blot analysis showed that BST-2 activated NF-κB by detecting total P65 and p-IkBα. (E) Western blot analysis showed that BST-2 affected ERK1/2 phosphorylation by the NF-κB signaling pathway. (F) qRT-PCR detected the mRNA levels of the anti-apoptosis factors Bcl-xL, CIAP2, FLIP, and livin in xenograft tumors. The results are reported as the mean ± SD of three independent experiments. ns, no significance.

important role in HBV-associated HCC. Western blotting was employed to unveil the change in BST-2 expression in HBV-associated HCC. We found that non-N-glycosylated BST-2 was aberrantly expressed in HBV-associated HCC tissues (*Figure 2*).

Glycosylation is the most prolific form of protein modification in mammalian cells (40). Accumulating evidence has shown that aberrant glycosylation frequently occurs in cancer (41,42). Alterations in glycosylation patterns regulate cancer development and progression, serve as important biomarkers, and provide a set of specific targets for diagnosis and therapeutic intervention. We and other groups have proved that N-glycosylation of BST-2 on Asn^{65} and Asn^{92} was dispensable for antiviral function, but was crucial for the folding, transport, and localization of BST-2 (28). The function of BST-2 N-glycosylation in NF-κB activation or even tumorigenesis is unclear. Oligosaccharyltransferase (OST) and EDEM1, 2, 3 are responsible for N-glycan synthesis and N-glycan trimming in the lumen of the ER, respectively (43,44). HBV proteins, including LHBs, HBx, and HBc, have been shown to induce ER stress in the liver (45). This stress could change

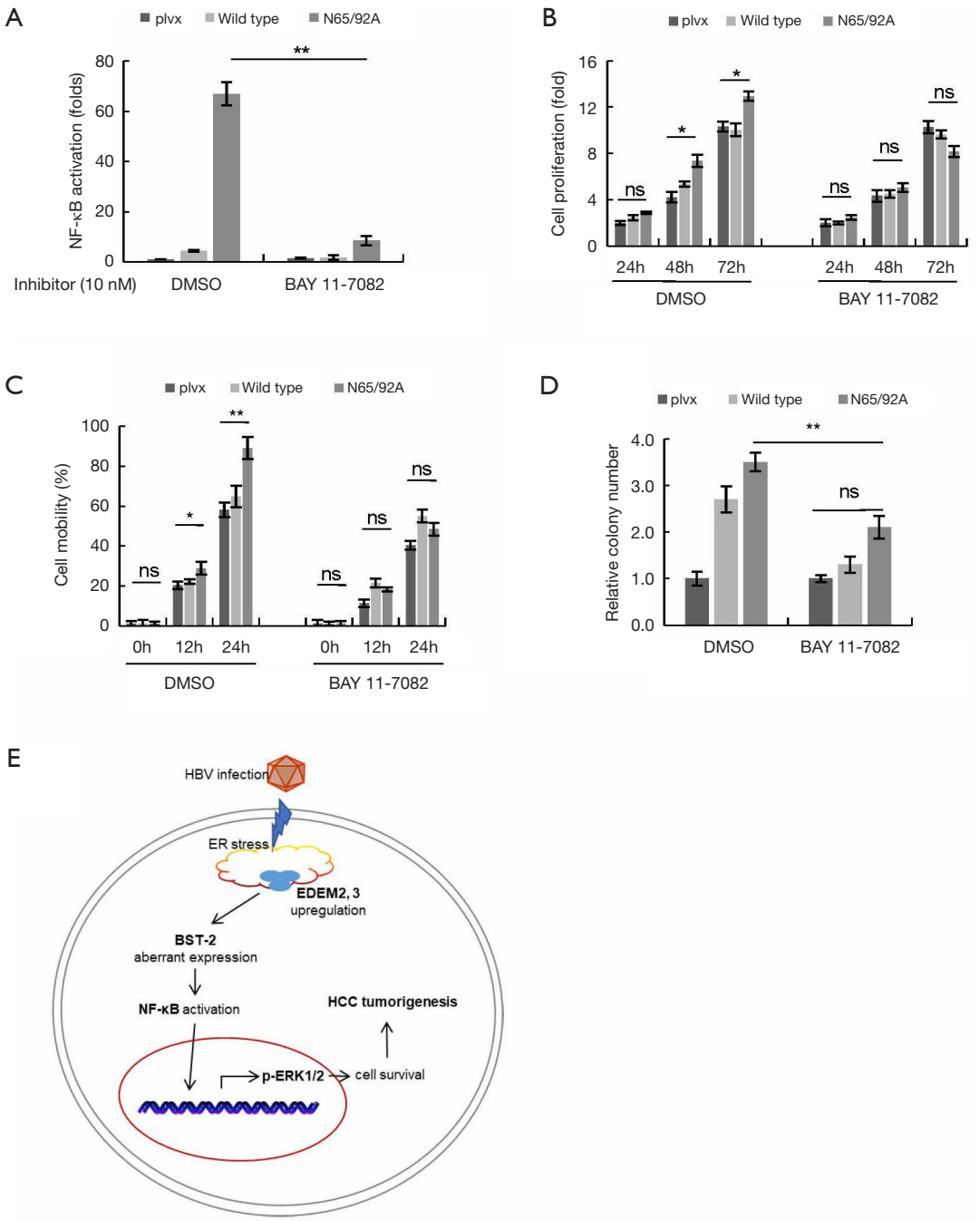

Figure 6 NF-κB inhibition attenuates the effect of BST-2 promoting HCC tumorigenesis in vitro. (A) Identification of the inhibition activity of BAY 11-7082 on NF-κB activation by dual-luciferase reporter assays. (B) Cell proliferation of BAY 11-7082-treated or untreated HepG2:WT, HepG2:N65/92A, and control cells was measured by CCK8 assays. (C) Cell migration of BAY 11-7082-treated or untreated HepG2:WT, HepG2:N65/92A, and control cells was measured by wound healing assays. (D) Colony formation of HepG2:WT, HepG2:N65/92A, and control cells was measured. (E) Logical model of BST-2 involves HBV-associated HCC by NF-κB/ERK axis. The results are reported as the mean ± SD of three independent experiments. ns, no significance; *, P<0.05; **, P<0.01.

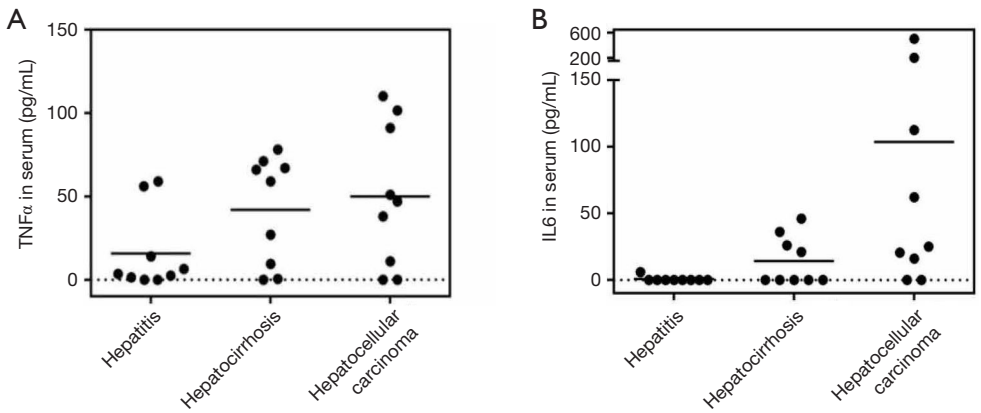

Figure 7 HCC-associated inflammatory cytokines TNFα (A) and IL6 (B) in the serum from 27 HCC patients following liver injury and disease progression were tested by ELISA.

the levels of OST and EDEMs, resulting in initial N-glycan synthesis and subsequent trimming of glycoproteins. Since non-N-glycosylated BST-2 was specifically expressed in HCC tissues (*Figure 2C*), we investigated N-glycosylation-related OST and EDEMs mRNA levels in paired HCC specimens. The mRNA of EDEM2 and EDEM3, but not OST (data not shown), showed higher expression in HCC tumors (*Figure 3*). Importantly, we proved that EDEM3 but not EDEM1 and 2 could trim the N-glycan of BST-2 to produce the non-N-glycosylated form (*Figure 3B*). And we demonstrated that HBV could increase the half-life of N-glycosylated deficient BST-2 (*Figure 3C*), hinting that HBV-induced retention of non-N-glycosylated BST-2 might has other function.

Since BST-2 retention on cell surface has been shown to activate the NF-κB (31,32), we detected the effect of WT and N-glycosylated deficiency mutants on NF-κB activation. The results demonstrated that non-N-glycosylated N65/92A showed stronger NF-κB activation compared to that of the WT (*Figure 5*). In addition, non-N-glycosylated BST-2 had stronger interaction with Syk than the WT, and is required for downstream NF-κB activation (*Figure 5C*). The excessive activation of NF-κB has been linked to inflammation and cancer, and it functions widely as a regulator of genes that control cell proliferation and cell survival (33,34). HCC-associated inflammatory cytokines TNFα and IL6 were tested and continuously increased due to NF-κB activation in the serum from 27 HCC patients following liver injury and disease progression (*Figure 7*). Li *et al.* proved that HBV MHBs enhance IL-6 production via the p38 MAPK/NF-κB pathway in an ER stress-dependent manner (46), which is consistent with the liver microenvironment in HBV-infected HCC patients. To ascertain the relationship between non-N-glycosylated BST-2 and HCC, WT and non-N-glycosylated mimic mutants of BST-2 were transfected and stably expressed in HCC cells. The ectopic expression of BST-2 promoted the characteristics of HCC cells *in vitro* (*Figure 4*), suggesting that BST-2 is sufficient and essential for HCC initiation and development. Except for the wound healing experiment, the WT BST-2 transfected cells showed obvious effects on tumorigenesis and development, which is consistent with previous reports (47,48). More importantly, the non-N-glycosylated mutant N65/92A exhibited a stronger effect on tumor promotion than WT BST-2. Furthermore, a mouse xenograft model confirmed that non-N-glycosylated BST-2 expression was conducive to xenograft growth *in vivo* (*Figure 4*).

NF-κB-mediated cell survival and opposition to apoptosis are two kinds of tumorigenesis pathways. Previous studies have reported that BST-2 could induce ERK and AKT phosphorylation to result in bladder cancer and activating Bcl-xL and livin to result in nasopharyngeal cancer (15,49). In our research, we confirmed that NF-κB/ERK1/2 pathway but not NF-κB/anti-apoptosis pathway (Bcl-xL, livin, FLIP, and CIAP2), were activated in mouse xenografts (*Figure 5*). The NF-κB inhibitor impaired the proliferation, migration, and colony formation of both BST-2 non-N-glycosylated mutant and the BST-2 WT-induced cells *in vitro* (*Figure 6*). Excessive upregulation of NF-κB/ERK might be a crucial method of BST-2-mediated HCC tumorigenesis.

Based on our research, we propose the following model of liver cancer cell survival (*Figure 6E*): HBV infection upregulates BST-2 expression and results in ER stress

which elevates the levels of EDEM3; EDEM3 induces aberrant expression of non-N-glycosylated BST-2; BST-2 and non-N-glycosylated BST-2 both activates NF-κB and consequently promotes the phosphorylation of ERK1/2, but non-N-glycosylated BST-2 activates more; the phosphorylation of ERK1/2 results in cell survival and HCC tumorigenesis. Our findings present a novel relationship between BST-2 and HBV-associated HCC. The upregulation of BST-2 in cancer cells could make it an attractive target for immunotherapy.

Acknowledgments

We thank the department of Biobank, division of clinical research of the first hospital of Jilin university for the providing of human tissues. We thank Springer Nature Author Services for the language editing (verification code DCAC-BC1F-A15F-CD7E-554F).

Funding: This work was supported by funding from the Chinese Ministry of Science and Technology (2018ZX10302104-001-010), the National Natural Science Foundation of China (81672004 and 31270202), Science and Technology Department of Jilin Province (20160101044JC and 20160101042JC), Health and Family Planning Commission of Jilin Province (2013Z066), the Key Laboratory of Molecular Virology, Jilin Province (20102209).

Footnote

Reporting Checklist: The authors have completed the ARRIVE reporting checklist. Available at http://dx.doi.org/10.21037/jgo-20-356

Data Sharing Statement: Available at http://dx.doi.org/10.21037/jgo-20-356

Conflicts of Interest: All authors have completed the ICMJE uniform disclosure form. All authors have no conflicts of interest to declare (available at http://dx.doi.org/10.21037/jgo-20-356).

Ethical Statement: The authors are accountable for all aspects of the work in ensuring that questions related to the accuracy or integrity of any part of the work are appropriately investigated and resolved. The study was conducted in accordance with the Declaration of Helsinki (as revised in 2013). The study was approved by the Ethics Review Boards of the First Hospital of Jilin University (No. 2016-255) and informed consent was taken from all individual participants. For any experiments involving animals, they were performed under a project license (No. 2016-320) granted by the Ethics Review Boards of the First Hospital of Jilin University, in compliance with Chinese national or institutional guidelines for the care and use of animals. All procedures used in the animal studies were approved by All animal experiments met the Animal Welfare guidelines.

References

1. Bray F, Ferlay J, Soerjomataram I, et al. Global cancer statistics 2018: GLOBOCAN estimates of incidence and mortality worldwide for 36 cancers in 185 countries. CA Cancer J Clin 2018;68:394-424. Erratum in: CA Cancer J Clin 2020;70:313.
2. Yang JD, Hainaut P, Gores GJ, et al. A global view of hepatocellular carcinoma: trends, risk, prevention and management. Nat Rev Gastroenterol Hepatol 2019;16:589-604.
3. Villanueva A. Hepatocellular Carcinoma. N Engl J Med 2019;380:1450-62.
4. Mahauad-Fernandez WD, DeMali KA, Olivier AK, et al. Bone marrow stromal antigen 2 expressed in cancer cells promotes mammary tumor growth and metastasis. Breast Cancer Res 2014;16:493.
5. Wang W, Nishioka Y, Ozaki S, et al. HM1.24 (CD317) is a novel target against lung cancer for immunotherapy using anti-HM1.24 antibody. Cancer Immunol Immunother 2009;58:967-76.
6. Mukai S, Oue N, Oshima T, et al. Overexpression of Transmembrane Protein BST2 is Associated with Poor Survival of Patients with Esophageal, Gastric, or Colorectal Cancer. Ann Surg Oncol 2017;24:594-602.
7. Goto T, Kennel SJ, Abe M, et al. A novel membrane antigen selectively expressed on terminally differentiated human B cells. Blood 1994;84:1922-30.

8. Ozaki S, Kosaka M, Wakatsuki S, et al. Immunotherapy of multiple myeloma with a monoclonal antibody directed against a plasma cell-specific antigen, HM1.24. Blood 1997;90:3179-86.
9. Walter-Yohrling J, Cao X, Callahan M, et al. Identification of genes expressed in malignant cells that promote invasion. Cancer Res 2003;63:8939-47.
10. Cai D, Cao J, Li Z, et al. Up-regulation of bone marrow stromal protein 2 (BST2) in breast cancer with bone metastasis. BMC Cancer 2009;9:102.
11. Yokoyama T, Enomoto T, Serada S, et al. Plasma membrane proteomics identifies bone marrow stromal antigen 2 as a potential therapeutic target in endometrial cancer. Int J Cancer 2013;132:472-84.
12. Mahauad-Fernandez WD, Borcherding NC, Zhang W, et al. Bone marrow stromal antigen 2 (BST-2) DNA is demethylated in breast tumors and breast cancer cells. PLoS One 2015;10:e0123931.
13. Sayeed A, Luciani-Torres G, Meng Z, et al. Aberrant regulation of the BST2 (Tetherin) promoter enhances cell proliferation and apoptosis evasion in high grade breast cancer cells. PLoS One 2013;8:e67191.
14. Ohtomo T, Sugamata Y, Ozaki Y, et al. Molecular cloning and characterization of a surface antigen preferentially overexpressed on multiple myeloma cells. Biochem Biophys Res Commun 1999;258:583-91.
15. Kuang CM, Fu X, Hua YJ, et al. BST2 confers cisplatin resistance via NF-κB signaling in nasopharyngeal cancer. Cell Death Dis 2017;8:e2874.
16. Jouvenet N, Neil SJ, Zhadina M, et al. Broad-spectrum inhibition of retroviral and filoviral particle release by tetherin. J Virol 2009;83:1837-44.
17. Andrew A, Strebel K. The interferon-inducible host factor bone marrow stromal antigen 2/tetherin restricts virion release, but is it actually a viral restriction factor? J Interferon Cytokine Res 2011;31:137-44.
18. Lazar C, Uta M, Branza-Nichita N. Modulation of the unfolded protein response by the human hepatitis B virus. Front Microbiol 2014;5:433.
19. Hirao K, Natsuka Y, Tamura T, et al. EDEM3, a soluble EDEM homolog, enhances glycoprotein endoplasmic reticulum-associated degradation and mannose trimming. J Biol Chem 2006;281:9650-8.
20. Chiang WF, Cheng TM, Chang CC, et al. Carcinoembryonic antigen-related cell adhesion molecule 6 (CEACAM6) promotes EGF receptor signaling of oral squamous cell carcinoma metastasis via the complex N-glycosylation. Oncogene 2018;37:116-27.
21. Mehta A, Herrera H, Block T. Glycosylation and liver cancer. Adv Cancer Res 2015;126:257-79.
22. Swiecki M, Omattage NS, Brett TJ. BST-2/tetherin: structural biology, viral antagonism, and immunobiology of a potent host antiviral factor. Mol Immunol 2013;54:132-9.
23. Lv M, Zhang B, Shi Y, et al. Identification of BST-2/tetherin-induced hepatitis B virus restriction and hepatocyte-specific BST-2 inactivation. Sci Rep 2015;5:11736.
24. Bustin SA, Wittwer CT. MIQE: A Step Toward More Robust and Reproducible Quantitative PCR. Clin Chem 2017;63:1537-8.
25. Vandesompele J, De Preter K, Pattyn F, et al. Accurate normalization of real-time quantitative RT-PCR data by geometric averaging of multiple internal control genes. Genome Biol 2002;3:RESEARCH0034.
26. Liu W, Cao Y, Wang T, et al. The N-Glycosylation Modification of LHBs (Large Surface Proteins of HBV) Effects on Endoplasmic Reticulum Stress, Cell Proliferation and its Secretion. Hepat Mon 2013;13:e12280.
27. Sasset L, Petris G, Cesaratto F, et al. The VCP/p97 and YOD1 Proteins Have Different Substrate-dependent Activities in Endoplasmic Reticulum-associated Degradation (ERAD). J Biol Chem 2015;290:28175-88.
28. Han Z, Lv M, Shi Y, et al. Mutation of Glycosylation Sites in BST-2 Leads to Its Accumulation at Intracellular CD63-Positive Vesicles without Affecting Its Antiviral Activity against Multivesicular Body-Targeted HIV-1 and Hepatitis B Virus. Viruses 2016;8:62.
29. Pikarsky E, Porat RM, Stein I, et al. NF-kappaB functions as a tumour promoter in inflammation-associated cancer. Nature 2004;431:461-6.
30. Haybaeck J, Zeller N, Wolf MJ, et al. A lymphotoxin-driven pathway to hepatocellular carcinoma. Cancer Cell 2009;16:295-308.
31. Galao RP, Le Tortorec A, Pickering S, et al. Innate sensing of HIV-1 assembly by Tetherin induces NFkappaB-dependent proinflammatory responses. Cell Host Microbe 2012;12:633-44.
32. Galao RP, Pickering S, Curnock R, et al. Retroviral retention activates a Syk-dependent HemITAM in human tetherin. Cell Host Microbe 2014;16:291-303.
33. DiDonato JA, Mercurio F, Karin M. NF-kappaB and the link between inflammation and cancer. Immunol Rev 2012;246:379-400.
34. Hoesel B, Schmid JA. The complexity of NF-kappaB

signaling in inflammation and cancer. Mol Cancer 2013;12:86.
35. Trepo C, Chan HL, Lok A. Hepatitis B virus infection. Lancet 2014;384:2053-63.
36. Ferlay J, Soerjomataram I, Dikshit R, et al. Cancer incidence and mortality worldwide: sources, methods and major patterns in GLOBOCAN 2012. Int J Cancer 2015;136:E359-86.
37. Van Damme N, Goff D, Katsura C, et al. The interferon-induced protein BST-2 restricts HIV-1 release and is downregulated from the cell surface by the viral Vpu protein. Cell Host Microbe 2008;3:245-52.
38. Radoshitzky SR, Dong L, Chi X, et al. Infectious Lassa virus, but not filoviruses, is restricted by BST-2/tetherin. J Virol 2010;84:10569-80.
39. Tokarev A, Suarez M, Kwan W, et al. Stimulation of NF-kappaB activity by the HIV restriction factor BST2. J Virol 2013;87:2046-57.
40. Zhao Y, Sato Y, Isaji T, et al. Branched N-glycans regulate the biological functions of integrins and cadherins. Febs J 2008;275:1939-48.
41. Tanaka T, Yoneyama T, Noro D, et al. Aberrant N-Glycosylation Profile of Serum Immunoglobulins is a Diagnostic Biomarker of Urothelial Carcinomas. Int J Mol Sci 2017;18:2632.
42. Magalhaes A, Duarte HO, Reis CA. Aberrant Glycosylation in Cancer: A Novel Molecular Mechanism Controlling Metastasis. Cancer Cell 2017;31:733-5.
43. Hosokawa N, Wada I, Hasegawa K, et al. A novel ER alpha-mannosidase-like protein accelerates ER-associated degradation. EMBO Rep 2001;2:415-22.
44. Ruiz-Canada C, Kelleher DJ, Gilmore R. Cotranslational and posttranslational N-glycosylation of polypeptides by distinct mammalian OST isoforms. Cell 2009;136:272-83.
45. Montalbano R, Honrath B, Wissniowski TT, et al. Exogenous hepatitis B virus envelope proteins induce endoplasmic reticulum stress: involvement of cannabinoid axis in liver cancer cells. Oncotarget 2016;7:20312-23.
46. Li YX, Ren YL, Fu HJ, et al. Hepatitis B Virus Middle Protein Enhances IL-6 Production via p38 MAPK/NF-kappaB Pathways in an ER Stress-Dependent Manner. PLoS One 2016;11:e0159089.
47. Yi EH, Yoo H, Noh KH, et al. BST-2 is a potential activator of invasion and migration in tamoxifen-resistant breast cancer cells. Biochem Biophys Res Commun 2013;435:685-90.
48. Mahauad-Fernandez WD, Okeoma CM. Cysteine-linked dimerization of BST-2 confers anoikis resistance to breast cancer cells by negating proapoptotic activities to promote tumor cell survival and growth. Cell Death Dis 2017;8:e2687.
49. Shigematsu Y, Oue N, Nishioka Y, et al. Overexpression of the transmembrane protein BST-2 induces Akt and Erk phosphorylation in bladder cancer. Oncol Lett 2017;14:999-1004.

Cite this article as: Zhang J, Zheng B, Zhou X, Zheng T, Wang H, Wang Y, Zhang W. Increased BST-2 expression by HBV infection promotes HBV-associated HCC tumorigenesis. J Gastrointest Oncol 2021;12(2):694-710. doi: 10.21037/jgo-20-356

Supplementary

Table S1 Information of primary antibodies used in this study

Antibody	Vendor	Catalog No.
BST-2	Proteintech	13560-1-AP
p65	Proteintech	10745-1-AP
IκBα	Cell Signaling Technology	9242S
p-IκBα	Cell Signaling Technology	9246S
AKT	BBI Life Science	D160001
p-AKT	BBI Life Science	D155156
ERK1/2	BBI Life Science	D160317
p-ERK1/2	BBI Life Science	D151580
β-tubulin	Beijing Ray Antibody Biotech	RM2003
HA tag	Invitrogen	71-5500
Myc tag	Millipore	05-724

Table S2 Oligonucleotides used for qRT-PCR

Gene	Oligonucleotides (5'→3')
BST-2	F: ACGCGTCTGCAGAGGTG
	R: GGCCCAGCAGCACAAT
GAPDH	F: TGCACCACCAACTGCTTAGC
	R: GGCATGGACTGTGGTCATGAG
EDEM1	F: TCCTTAAAGGGGAAGCGAGCC
	R: AGCGCTCGCCATTGCATGGT
EDEM2	F: AGTGGTTGAAGTGCTCCAGGA
	R: CAGCCTCTACTTCCACCCCA
EDEM3	F: GGCTTGGTGGCTTCGGGAAA
	R: ACATTGCTGGACGCTGGTGG
Bcl-xL	F: CGTGGAAAGCGTAGACAAGGA
	R: AGAGTGAGCCCAGCAGAACC
CIAP2	F: CTTTTGCTGTGATGGTGGACTC
	R: TCTCCTGGGCTGTCTGATGTG
FLIP	F: ACCCTCACCTTGTTTCGGACT
	R: TGCCTCGGCCCATGTAAT
Livin	F: GTCAGTTCCTGCTCCGGTCA
	R: GCTGCGTCTTCCGGTTCTT
β-Actin	F: ACCGAGCGCGGCTACAG
	R: CTTAATGTCACGCACGATTTCC
HMBS	F: GGCAATGCGGCTGCAA
	R: GGGTACCCACGCGAATCAC

http://dx.doi.org/10.21037/jgo-20-356

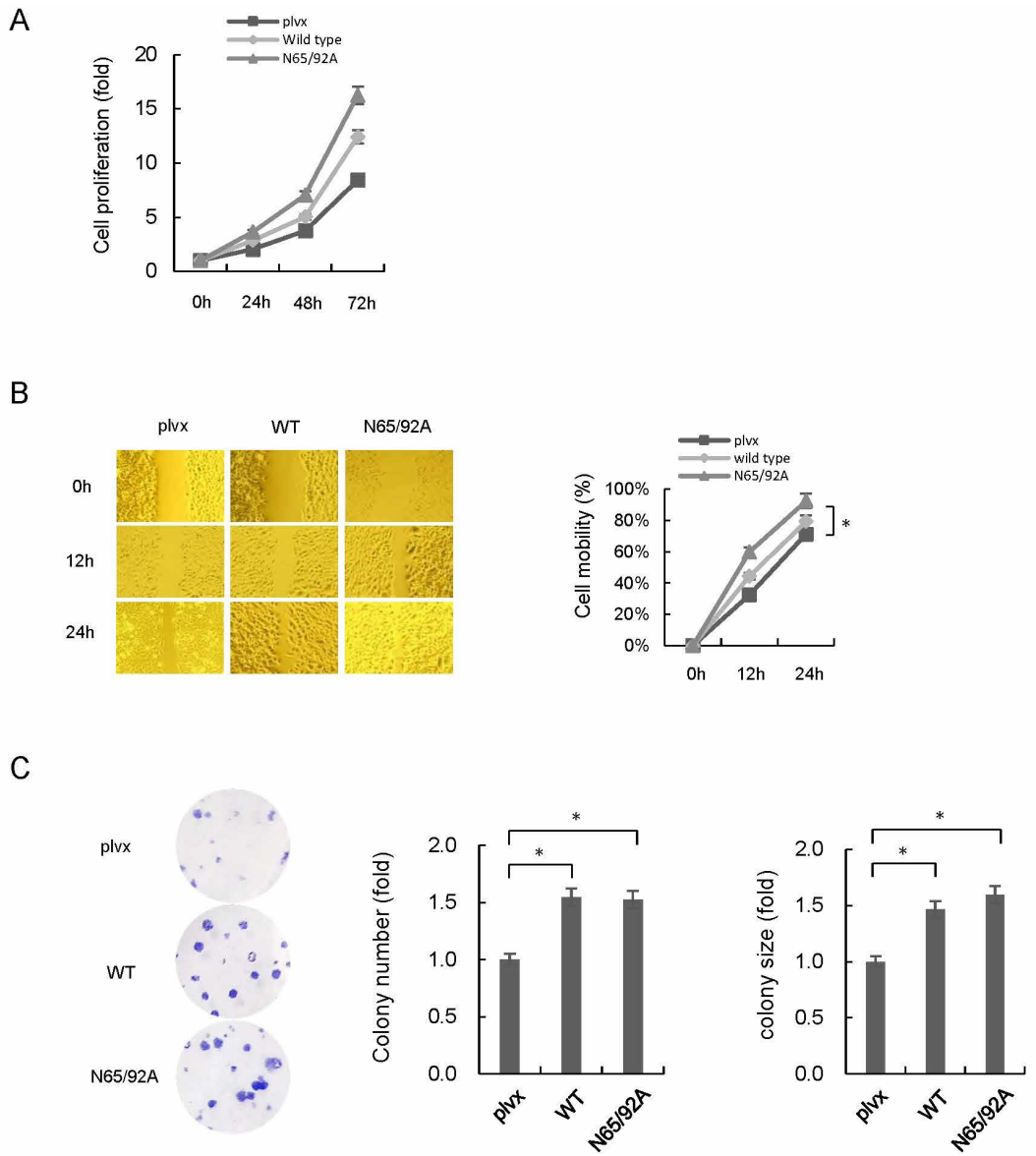

Figure S1 N-glycosylation of BST-2 involves HCC tumorigenesis in L02 cells. (A) Cell proliferation of L02:WT, L02:N65/92A, and control cells was measured by CCK8. (B) Cell migration of L02:WT, L02:N65/92A, and control cells was measured and quantified by wound healing assays. (C) Colony formation of L02:WT, L02:N65/92A, and control cells was measured and quantified. The results are reported as the mean ± SD of three independent experiments. ns, no significance; *, P<0.05; **, P<0.01.

http://dx.doi.org/10.21037/jgo-20-356